Ion beam sputtering nanopatterning of thin metal films: the synergism of kinetic self-organization and coarsening

M Stepanova[1,2] **and S K Dew**[2]

[1] National Institute for Nanotechnology NRC, Edmonton, AB, Canada
[2] Department of Electrical and Computer Engineering, University of Alberta, Edmonton, AB,
Canada

Abstract
Creation of self-organized surface nanostructures by ion beam sputtering (IBS) has strong
potential for use in a broad range of technologies, from nanoelectronics and photonics to
sensing and catalysis. Recently, we have developed a simple two-stage process for fabricating
self-assembled arrays of Cu dots and lines on Si and SiO_2 substrates employing IBS of thin Cu
films. We found that the self-assembled structures on the substrate result from a complex
interaction between the structure-forming kinetic instability and various outcomes of the surface
diffusion and coarsening, which tend to drive the surface pattern towards a thermodynamic
equilibrium. Here, we analyze in detail the interplay of the kinetic nanopatterning and
coarsening, in order to better understand the mechanisms defining the IBS-generated metallic
structures on substrates of a different material. By means of kinetic Monte Carlo (KMC)
modeling we investigate the pertinent trends of the self-organization at the surface of a metallic
film. In the light of this discussion, we review the fabricated nanostructures. Finally, we present
a KMC model of the two-stage IBS process and analyze the stability of the fabricated metal
patterns at the surface of a substrate. We discuss the opportunities and challenges of this
technique, concluding that the IBS creation of surface heterostructures provides considerable
room for future numerical and experimental studies.

1. Introduction

Nanostructured surfaces have a strong potential for applications in a broad range of technologies, from nanoelectronics and photonics to sensing and catalysis. Methodologies employing self-organized formation of such nanostructures [1] are of a special interest since they are relatively simple and cost-efficient in comparison with direct-write techniques, such as optical and electron beam lithography. The potential of ion beam sputtering (IBS) to generate self-assembled surface patterns as a result of kinetic instability [2] has raised a significant enthusiasm over the last decade [3–6]. In brief, when a solid surface is exposed to a beam of atomic particles, these deposit their energy at the surface. Some of the surface atoms that have received the deposited energy are emitted (sputtered). The overall amount of deposited energy (and therefore the number of emitted atoms) is sensitive to the surface curvature. Atoms are emitted preferentially from hollows, whereas

emission from tops of mounds is inhibited, which leads to self-organized nanoscale morphologies.

The capabilities to control self-assembled surface nanostructures by varying the bombardment conditions have been addressed extensively in the literature [7–24]. Experiments [5, 8, 13, 14, 16–18, 22–24] have shown that the angle of the ion incidence is one of primary factors determining the surface morphology, which is usually composed of hillocks at normal incidence, whereas oblique incidence can generate arrays of quasi-periodic ripples. The most often encountered in experiments are parallel and normal orientations of the ripples with respect to the projected beam direction, depending on bombardment conditions. This sensitivity of the self-assembled morphology to the bombardment conditions is consistent with the theory [2, 7, 9–11, 21] and kinetic Monte Carlo (KMC) modeling [12, 17–20, 22].

Besides the shape and orientation of the self-organized morphologies, predictability of the features' sizes and

positions is another major point of importance for applications. According to linear theory [2], the size of sputter-induced nanostructures is defined by the distributions of energy deposited by incoming ions, and also by the surface diffusivity, which suggests that a characteristic size of the surface structures can be identified. However, some of observed surface morphologies tend to coarsen during ion bombardment [3, 5, 15, 23], indicating that there is no one well-defined characteristic size. A moderate coarsening of surface nanostructures has been captured by recent theory [21] and KMC simulations [19, 22] of sputtering. Experiments, however, indicate that coarsening may be stronger than these models predict, in particular during sputtering of (poly)crystalline films and in metallic films deposited on some non-metallic substrates [5, 15, 17, 25].

Being capable to fabricate, in a controllable fashion, IBS-generated nanostructures on substrates of another material is of a major interest for potential applications of ion beam nanopatterning. In particular, arrays of metal nanodots on non-metallic substrates present a considerable interest as nonlinear electronic nanodevices [26–28] and storage nodes for nanocrystal memories [29, 30]. Some metal nanodots and nanosize metallic lines (nanowires) exhibit diverse nonlinear properties [31–34]. Recently, we have developed a simple two-stage process to fabricate self-assembled arrays of Cu dots and lines on Si and SiO$_2$ substrates employing sputtering of thin metallic films by an ion beam [17, 18, 22]. We found that the self-assembled structures on the substrate result from a complex interaction between the structure-forming kinetic instability and various outcomes of the surface diffusion and coarsening, which tend to drive the surface pattern towards a thermodynamic equilibrium. For the potential of the IBS fabrication of surface heterostructures to be fully realized, both the kinetic self-organization and the coarsening processes should be understood in detail [5, 11].

In this paper, we analyze the impact of kinetic nanopatterning and coarsening, in order to better understand the mechanisms defining sputter-generated metallic structures on substrates of a different material. In section 2 we consider the pertinent trends of the kinetic self-organization at the surface of a continuous metal film, as predicted by our KMC modeling [17, 18, 22]. In section 3, we provide an overview of nanostructures on substrates, which we have fabricated by the two-stage technique [17, 18, 22], and discuss these results in the light of predicted trends. In section 4, we present a KMC modeling of the two-stage fabrication process [17, 25], and analyze the stability of the fabricated metal patterns at the surface of a substrate. Section 5 summarizes our conclusions and outlines a path for further creation of surface heterostructures by sputtering of thin metallic films.

2. Encouraging insight from KMC modeling

In this section, we analyze numerically the trends of surface nanopatterning, for the example of Cu films exposed to 1 keV Ar ion bombardment. For this purpose, we employ our KMC model that we have reported earlier in [17, 18, 22]. The model accounts for two major factors defining the
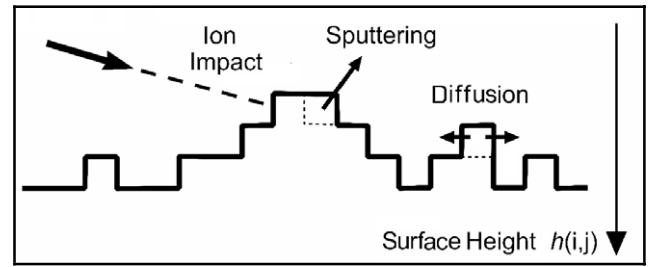

Figure 1. The model of ion beam sputtering and surface diffusion.

surface morphology, e.g. sputtering of surface atoms due to energy deposition by the ions, and thermally activated surface diffusion. The model has proven to match closely both the size and lateral shape of experimentally observed surface nanostructures [18, 22].

Figure 1 outlines the model. We describe the surface by a height function $h(i, j)$, where $\{i, j\}$ denote atom-sized cells of a two-dimensional rectangular 440×440 grid with periodic boundary conditions, representing an approximately 100 nm $\times$ 100 nm surface fragment. When an atom is removed or added at a cell $\{i, j\}$, the height $h(i, j)$ changes by one atomic size. Incident Ar atoms are generated at random positions above the surface and their impact points are defined as shown in figure 1. Such an impact mechanism naturally accounts for shadowing of Ar trajectories by surface morphology, which leads to screening out some surface regions [12, 13, 22]. Upon reaching the surface, the Ar ions are either reflected with the probability dependent on the local angle of incidence [18, 35] or penetrate inside the surface and deposit their energy into a volume of ellipsoidal shape. The spatial distributions of deposited energy match the shape and size of the collision cascades generated by 1 keV Ar ions in Cu [18, 22]. After each energy deposition event, surface atoms are removed at a probability based on the sputtering yield, and computed through our improved formalism that is dependent on local angle of incidence [18, 13].

Bombardment creates surface adatoms, whose diffusion is also very important since it offsets amplification of short-wavelength noise and by this leads to formation of morphologies with a finite characteristic size. In our KMC model we employ a reversible, thermally activated diffusion process [17, 18, 22]. At each diffusion step, a cell $\{i, j\}$ and one of its neighbors $\{m, n\}$ are chosen randomly. The initial atomic configuration at the cell $\{i, j\}$ is characterized by an energy function E proportional to the average local curvature κ [17, 18], $E = 0.5a\gamma(|\kappa(i, j)| + |\kappa(m, n)|)$, where a is the cell size and $\gamma = 0.07$ eV is the energy of one bond [36]. With such a choice of E, in equilibrium are flat facets of every orientation with a constant local slope, which is more realistic than exclusively horizontal equilibrium facets supported by algorithms employed in earlier models [37]. Since the surface curvature κ is derived from local atomic configurations [18], the model is representative of most single-atom jump mechanisms contributing to the surface diffusion. The model is also capable to describe anisotropies of the surface diffusion [5] by employing direction-dependent
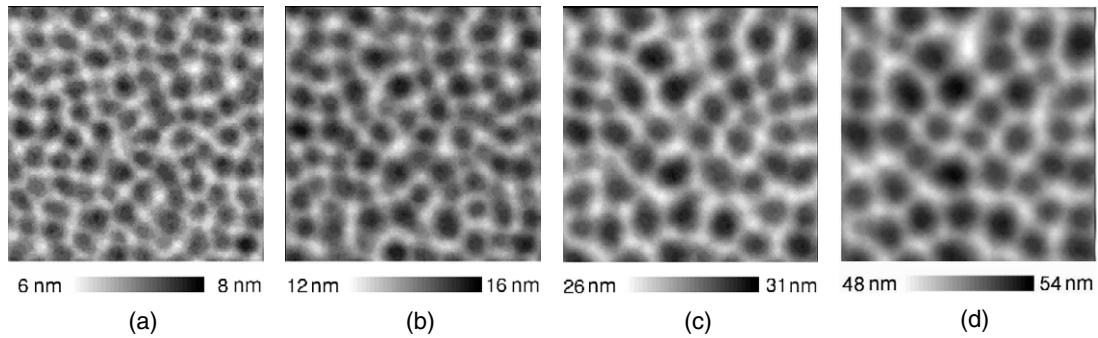
Figure 2. Simulated 100 nm × 100 nm surface morphologies for Cu bombarded by 1 keV Ar$^+$ ions at normal incidence, $\rho = 0.6 \times 10^4$, and various removed depths. The legend bars show the removed depth.

energies γ. In this study, however, a single average bond energy value has been adopted for compatibility with the quasi-isotropic structure of metallic films prepared by standard PVD techniques [18, 22]. Furthermore, the model is capable to describe the temperature dependence of the surface mobility. Thus, a jump $\{i, j\} \rightarrow \{m, n\}$ leads to the change $\Delta E = E_2 - E_1$, where '1' and '2' denote the configurations before and after the jump, respectively. The jump is accepted according to the Metropolis algorithm, e.g. with the probability $P = 1$ for $\Delta E \leqslant 0$ and with the probability $P = \exp(-\Delta E/kT)$ for $\Delta E > 0$. The latter probability is temperature dependent, and describes thermally activated jumps. However, in this work we consider the standard ion milling conditions at room temperature. We describe the surface mobility with the number of jump steps per one sputtering event, which we denote as the kinetic rate $\rho = I_{\mathrm{diff}}/I_{\mathrm{ion}}Y$. Here I_{diff} is the number of the Monte Carlo diffusion steps per cell, I_{ion} is the number of the ion impact steps per cell over the same simulation period, and Y is the corresponding average sputtering yield. By definition, $I_{\mathrm{diff}} = 4a^{-2}Dt$ and $I_{\mathrm{ion}} = a^2 J_0 t$, where t is time, D is the average surface diffusivity of Cu adatoms, and J_0 is the Ar flux. Thus, the kinetic rate can also be defined by $\rho = 4D/J_0 Y a^4$, and thus related to the relevant experimental conditions[3].

Figures 2(a)–(d) show typical simulated surface morphologies after the removal of ≈ 7 nm, ≈ 14 nm, ≈ 28 nm, and ≈ 52 nm, respectively, at normal incidence of the ion beam. The images correspond to the kinetic rate $\rho = 0.6 \times 10^4$, which is compatible with the standard ion milling regimes for VLSI fabrication employing ion fluxes of $\sim 10^{15}$ cm^{-2} s^{-1} [17, 18] (see footnote 3). It can be seen that the surface is covered by small hillocks which have formed a network of ring-like patterns. The corresponding height–height correlation functions $C(r, s) = \sum (h(x, y) - \bar{h})(h(x + r, y + s) - \bar{h})$ show clearly defined minima followed by maxima (see an example in figure 3) indicating that the patterns can be described by a characteristic distance d between hillocks. However, in contrast to the linear theory predicting one well-defined characteristic size of the morphology, in our simulations the surface pattern can coarsen by coalescence of the hillocks. This results in an $\sim 40\%$ increase of the average distance d during the

---

[3] Following our previous works [17, 18, 22], in most examples the magnitude of the diffusion rate is selected to match the surface diffusivity $D_{\mathrm{Cu}} \sim 10^{-12}$ cm^2 s^{-1} and the experimentally relevant ion fluxes through the surface, $J_0 \sim 10^{15}$ cm^{-2} s^{-1}.
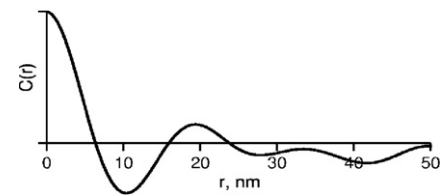
Figure 3. The height–height correlation function for the surface pattern in figure 2(d).
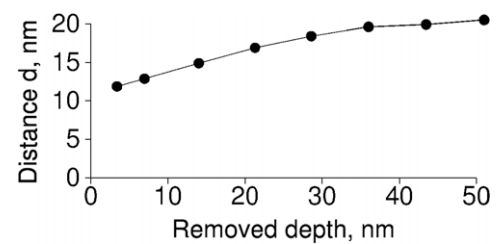

Figure 4. The average distance d between the hillocks of the Cu surface structure as a function of the average removed depth. The simulation parameters were the same as in figure 2. Adapted from [18].

initial stages of sputtering, as shown in figure 4. After approximately 35 nm are removed, the distance d stabilizes at the level of ≈ 20 nm, and changes only slightly in the course of further sputtering.

At oblique angles of ion incidence, the networks of hillocks lose their lateral symmetry [22]. At grazing angles of incidence (larger than approximately 70°), the pattern becomes an array of ripples directed along the surface projection of the Ar beam. Figure 5 presents an example of the evolution of such ripples generated by 80° incident Ar ions. It can be seen that, in agreement with published experiments [5, 8, 16], the simulated ripples have defects such as broken, merged, and bent lines. Elsewhere [22] we have suggested that these defects originate from the initial stage of sputtering, when the process of self-organization is not spatially correlated enough. The stochastic nature of sputtering results in multiple defects seen in the simulated morphologies at early stages of the process (see figure 5(a)). In the course of subsequent sputtering, some of the ripples coalesce resulting in moderate coarsening of
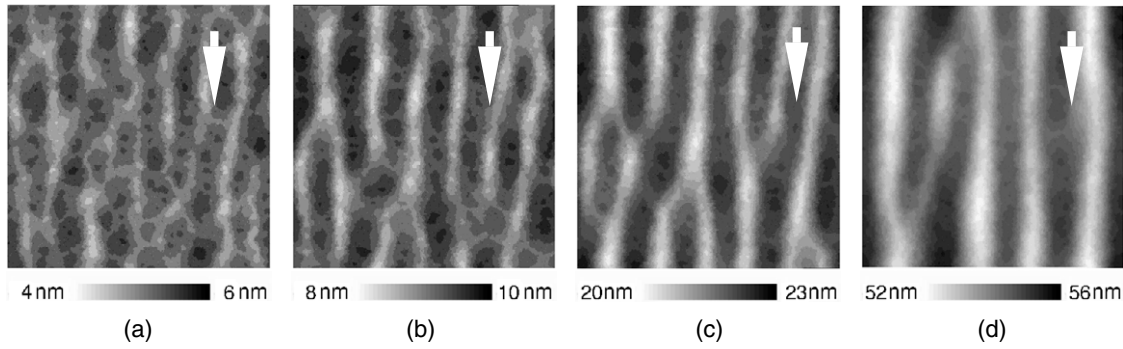
Figure 5. Simulated 100 nm × 100 nm surface morphologies for Cu bombarded by 1 keV Ar$^+$ ions at 80° incidence, $\rho = 2.3 \times 10^4$, and various removed depths. The legend bars show the removed depth, and the arrows indicate the direction of the ion beam.

the pattern, as can be seen in figures 5(b)–(d). A remarkable behavior evident from figure 5 is that the coalescence tends to eliminate defects in the pattern, making the ripples more uniform at later stages of etching. Similarly to the inter-feature distance in the network-like morphologies that develop at normal incidence, the average inter-ripple distance increases by approximately 40% at the beginning of sputtering. After 30–40 nm are removed, most defects are eliminated, and the average inter-ripple distance stabilizes.

The trend of the average distance between the hillocks (at near-normal incidence) and ripples (at oblique incidence) to saturate after a certain duration of sputtering indicates that in these examples the kinetic process of self-organization is the dominant one. Accordingly, a characteristic distance between the surface features can be identified for these patterns. In figure 6, this distance is presented a function of the kinetic rate, ρ. The dependencies for the patterns corresponding to the normal and grazing incidence of ions are reasonably matched by the power dependencies $d = 12.1\,a\rho^{0.22}$ and $d = 7.0a\rho^{0.26}$, respectively, where $\rho = 4D/J_0Ya^4$. Thus, the average distance d decreases approximately twice when the ion flux J_0 increases by an order of magnitude[4], at the condition that the bombardment-induced surface heating does not lead to a significant increase in the diffusivity D. It should be noted that the dependencies in figure 6 have been obtained for a constant (ambient) temperature T, and for the isotropic surface diffusion described by a single average bond energy γ. Varying the temperature and considering anisotropic or configuration-dependent jump energetics may affect the surface geometry, so that it is early to conclude, whether the power dependencies in figure 6 provide a universal trend. However, the dependencies are representative of the process that we address in this paper, e.g. IBS nanostructuring of deposited, quasi-isotropic metallic films at room temperature.

In conclusion, our simulations demonstrate the following:

- The angle of incidence of the Ar ion beam determines the geometry of the nanostructures on Cu surface. At normal incidence, the surface pattern is shaped as network of
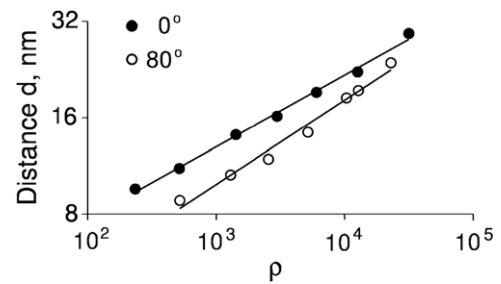

Figure 6. The average distance d between hillocks (normal ion incidence) and ripples (80° incidence) after removal of ~50 nm, as a function of the kinetic rate $\rho = 4D/J_0Ya^4$. The straight lines show the dependencies $d = 12.1\,a\rho^{0.22}$ and $d = 7.0a\rho^{0.26}$, respectively.

partially interconnected hillocks, whereas arrays of ripples directed along the surface projection of the Ar beam self-assemble under grazing incidence by the ions.

- The bombardment-induced surface features have shown a trend to coalesce resulting in a moderate coarsening at the initial stages of sputtering.

- Remarkably, coarsening does not distort the correlation in the surface patterns. Moreover, for grazing ion incidence it even results in more uniform ripples with fewer defects. After 30–40 nm are removed, depending on the simulation conditions, the inter-feature distance tends to stabilize and becomes insensitive to variations in the duration of sputtering. In these regimes the morphologies can be characterized by a well-defined inter-feature distance, indicating that the kinetic mechanism of surface nanostructuring is the dominant one in these examples.

- The size of the surface features shows a pronounced dependence on the ion flux J_0. Accordingly, changing the beam current would be a straightforward way to manipulate the size of the surface nanostructures, provided that appropriate temperature control is available in the sample, and the surface diffusivity does not increase significantly.

The predicted trends imply that ion beam sputtering might offer a significant level of control over the shape, orientation, and size of surface nanostructures. This motivates broadening

---

[4] This dependence is weaker than predicted by the linear theory [2], after which $d \sim (D/J_0Y)^{0.5}$. The disagreement apparently results from limitations of the theory, which is restricted to the first-order linear accounting for the surface curvature.
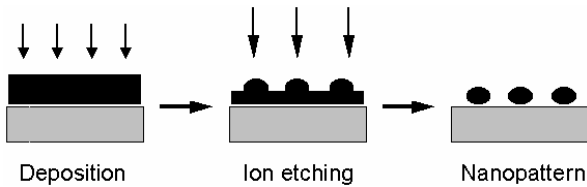
Figure 7. Fabrication of self-assembled metal nanostructures on Si and SiO$_2$ substrates.

the applications of the IBS nanopatterning, by trying to fabricate self-assembled nanostructures on a surface of another material. In section 3, we describe our achievements as well as difficulties that we have encountered when fabricating nanoscale heterostructures on substrates.

3. Realities of practical nanofabrication

In [17, 18, 22], we have developed a simple two-stage process to fabricate self-assembled arrays of metal islands and lines on Si and SiO$_2$ substrates. The process employs standard ion mill conditions and can be easily integrated with established VLSI technologies. This technique is outlined in figure 7. A thin layer of Cu ($\approx$50 nm) is deposited on the surface of Si and SiO$_2$ substrates and etched by a neutralized Ar beam until the Cu/Si substrate is reached. The surface nanopattern is imaged by SEM at various stages of this process.

For substrates, we used prime Si(100) wafers and 0211 glass wafers. The substrates were cleaned in hot solution 75% H$_2$SO$_4$:25% H$_2$O$_2$ for 15 min. Cu films were deposited on the substrates with a Lesker magnetron sputtering system using 99.995% Cu sputter targets. The system power and voltage were maintained at 150 W and 440 $\pm$ 10 V, respectively, and the base pressure in the chamber was less than 1.6×10^{-6} Torr. Using the system calibration and profilometric measurements, we have estimated the thickness of the deposited Cu films to be 50 $\pm$ 7 nm. The deposited Cu films were continuous and without significant roughness (see figure 8(a)). The samples were etched with an Oxford IonFab-300 ion mill facility. The base pressure in the chamber did not exceed 5×10^{-7} Torr. We employed a 1.2 keV neutralized Ar beam incident along the surface normal and at approximately 82° with respect to the normal. The Ar fluxes through the sample surface were $J_0 = 5 \times 10^{15}$ cm^{-2} s^{-1} and $J_0 = 1.4 \times 10^{15}$ cm^{-2} s^{-1}, respectively.

The ion mill system was equipped with a cooling supply that maintained the sample holder temperature below 27 °C in the process of etching. For characterization, we employed a JEOLs JSM6301FXV scanning electron microscope at a primary voltage of 5 keV.

Figures 8(b)–(d) show typical surface patterns for Cu on glass after sputtering at normal ion incidence, shown at various image resolutions. Clearly seen is a light network-like Cu pattern on a darker background that represents the substrate. Because of the network structure, the nanopattern is conductive and allows straightforward SEM imaging. A slightly longer etching time decreases the conduction to the level that SEM images cannot be taken, which confirms that we observe a Cu pattern on the substrate. Visible in figure 8(b) are a few $\approx$50 nm wide dark areas without copper. We attribute these to occasional depressions in the thickness of the deposited Cu layer, where copper was etched off earlier. The majority of the surface, however, is covered by tiny $\approx$25 nm wide ring-like Cu features, whose shape and size resemble the simulated morphologies in figure 2. From SEM imaging at an acute takeoff angle, we discerned that the Cu features are slightly raised over the substrate and their height is less than $\approx$10 nm. Our Fourier analysis [18] did not detect any long-range order or preferential orientations.
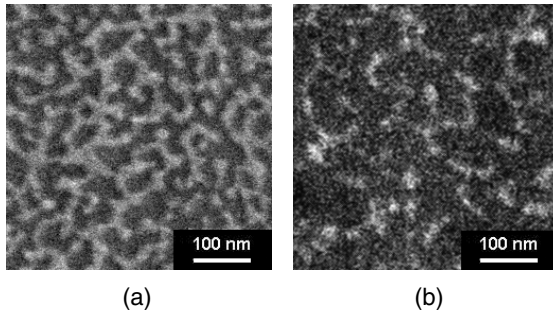
The Cu pattern on Si generated by normally incident Ar beam (figure 9(a)) is different. The pattern has coarsened significantly, and is shaped as a percolation network with the characteristic size of approximately 40–50 nm. With continuing etching, the network shrinks into elongated clusters (figure 9(b)). The size of the observed features is at least twice that predicted numerically in section 2.

Figures 10(a) and (b) show the Cu patterns on glass and Si, respectively, generated at the grazing incidence of the ion beam. It can be seen that arrays of Cu lines are formed on both substrates, and these arrays are similar in size, shape, and orientation. Thus, the difference in composition and crystalline structure of the substrate does not appear to cause a difference in these patterns. In agreement with our numeric modeling, the Cu lines are directed along the surface projection of the beam. The average inter-line distance, which is close to 30 nm, is compatible with the numeric results.

We found that choice of the ion energy is important for our process. Thus, when the energy is higher than 2 keV, ion bombardment of a Cu film generates an intense ballistic mixing
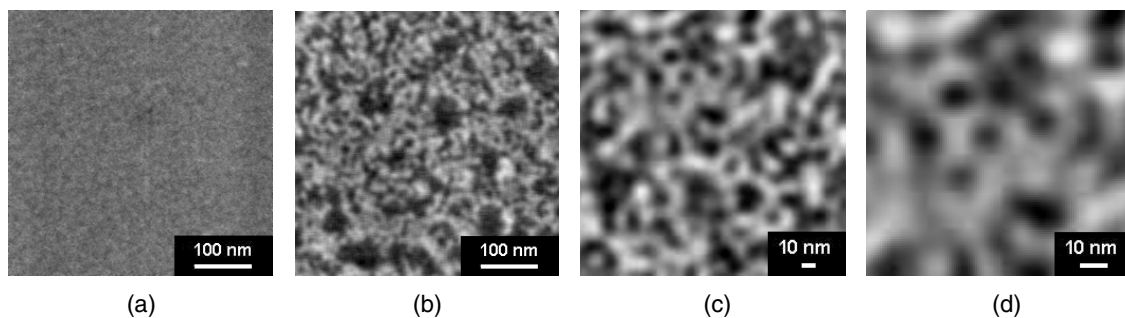
Figure 8. SEM images of as-deposited Cu film (a) and Cu nanopatterns on glass generated by normally incident 1.2 keV ions ((b)–(d)) at various image resolutions [18]. In ((b)–(d)) the light features represent Cu and the dark background represents the substrate.

Figure 9. SEM image of Cu network on Si generated by normally incident 1.2 keV ions (a). A slightly longer etching results in features with less Cu (b). The light features represent Cu and the dark background represents the substrate.
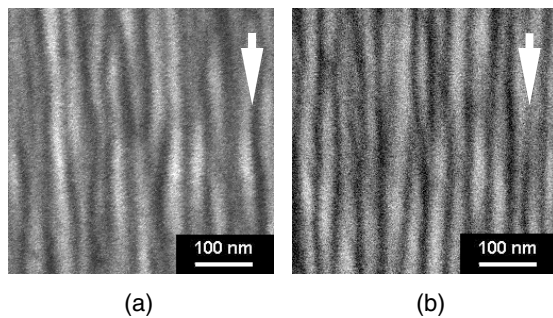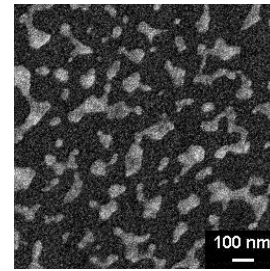

Figure 10. SEM image of Cu lines on glass (a) and Si (b) for grazing incidence of 1.2 keV ions [22]. The arrows show the projection of the ion beam at the surface.

Figure 11. SEM image of Ag pattern on Si, bombarded at normal ion incidence. The light features show Ag and the dark background represents the Si substrate.

with the substrate, which may lead to fuzzy patterns without clear boundaries or pronounced structure [25]. On the other hand, choosing the ion energy significantly below 1 keV leads to a dramatic decrease in the sputtering yield, which increases the etch time making the process inefficient. Thus, the 1–2 keV regimes appear to be the optimum for Cu.

In addition to Cu, we also attempted a similar process with Ag films. We have employed both Si and glass substrates, varied the ion energies in 1–3 keV regimes, and attempted various angles of ion incidence. However, only very coarse percolation patterns and islands were obtained with feature sizes of 100–200 nm and larger. A typical example for the coarse Ag islands is given in figure 11. Apparently, all correlation with the bombardment-induced pattern is lost in this case.

To summarize:

- Ion etching of thin Cu films by ≈1 keV ions at grazing incidence generates arrays of Cu lines that are basically similar on glass and crystalline Si substrates. There also is a close similarity between the fabricated patterns and those obtained numerically from KMC modeling. The lines' orientation is entirely controllable since they follow the projection of the Ar beam on the surface.
- Etching of Cu films on glass by normally incident ions provides network-like Cu patterns, which also resemble closely the corresponding numeric results by KMC.

- In contrast, Cu networks on Si substrates generated by normally incident ions have coarsened significantly. Coarsening becomes even more dramatic when Cu is replaced by Ag. In these samples, coarsening seems to destroy all correlation with the surface patterns generated by the ion bombardment.

We expect that the observed decline from the behaviors predicted by KMC in some of our samples is related to the impact of the boundaries separating the metal features and the substrate. Thus, clusters of poor silicide formers such as Cu and Ag would tend to coarsen to decrease the excess energy of their boundaries [38–40]. This suggests that IBS of thin metal films on substrates has two stages. At the first stage, the deposited metallic film is ion bombarded, and the corresponding surface pattern is generated as described in section 2. This occurs until the etched surface approaches the metal/substrate interface, the film losses its continuity, and metallic islands are formed on the substrate. At the second stage, the interface coarsening tends to increase the islands' size and minimize the overall length of their boundaries, whereas sputtering makes the islands shrink. In section 4, we investigate in detail the cooperative effect of sputtering and coarsening on metallic clusters at substrates.

4. Can interface coarsening be avoided?

We describe coarsening of metal patterns on substrates by a KMC model that we have introduced in [17, 25]. As a first step, we convert the predicted bombardment-induced morphology as described in section 2 into an array of metal islands on the substrate. Next, we simulate the cooperative effect of the interface coarsening and sputtering. We suggest that the resulting metal islands are, in general, more than one monolayer in height but have a 1 ML perimeter. To account for sputtering, we consider shrinkage of metal islands as outlined in figure 12. Although sputtering removes atoms from the entire surface of islands, only removals from the 1 ML perimeter are relevant to describe the shrinkage. At each Monte Carlo sputtering step, one surface cell is selected randomly; if the cell belongs to an island perimeter or is filled with an unbounded metal adatom, the adatom is removed. We describe sputtering by the average number of sputter steps per cell, I_{sp}.

The interface coarsening can be described by the traditional model of Ostwald ripening [38–40]. Accordingly to
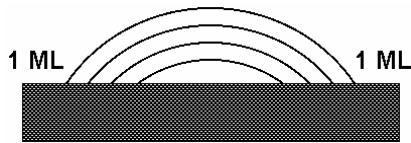
Figure 12. The model of metal island shrinkage by sputtering.

this mechanism, metal adatoms can detach from their locations at islands' perimeter and diffuse over the substrate until they are caught at another perimeter location, leading to competitive cluster growth. At each Monte Carlo step two nearest-neighbor cells, 1 and 2, are chosen randomly. If cell 1 contains an adatom and cell 2 does not, the probability of the jump from 1 to 2 is defined by the Metropolis algorithm with the energy function that depends on the number of nearest neighbors n, $E = -\gamma n$ for $n > n_c$ and $E = 0$ for $n \leqslant n_c$. Here γ is the energy of one adatom–adatom bond, and $n_c = 3$ is the critical number of neighbors. Following classic nucleation theory [41, 42], the number n_c identifies whether the adatom is linked to its neighbors by attractive bonds ($E < 0$), or it has been detached ($E = 0$). The Metropolis algorithm provides the jump probability $P = 1$ for $n_1 < n_2$ or $n_1 \leqslant n_C$, and $P = \exp(\gamma(n_2 - n_1)/kT)$ for $n_1 > n_2$ and $n_1 > n_C$. As a result, unbounded adatoms ($n \leqslant 3$) perform a random walk over the surface, whereas adatoms incorporated into stable islands ($n > 3$) jump preferentially into those positions that increase the number of their bonds with neighbors. This favors detachment of adatoms from island corners, in comparison to adatoms located at flat boundaries. As a result, larger islands with fewer corners per unit perimeter grow at the expense of smaller ones. At the conditions when Ostwald ripening interplays with sputtering, the overall metal coverage decreases with time, whereas particular islands can increase in size. We describe the proportion between the number of the surface diffusion steps I_{diff} and sputter steps I_{sp} by the kinetic rate parameter, $\rho_s = I_{\mathrm{diff}}/I_{\mathrm{sp}}$, whose meaning is, basically, similar to the kinetic rate ρ introduced in section 2. As previously, the kinetic rate can be defined by $\rho_s = 4D_s/J_0 Y a^4$, where D_s is the diffusivity of metal adatoms over the substrate, J_0 is the ion flux, and Y is the average sputtering yield for Cu. Since the diffusivities of Cu adatoms on Si and glass are unknown, we have employed model values of the kinetic rate within approximately the same regimes as in section 2.

Figure 13 shows the initial pattern obtained by the conversion of the surface structure from figure 2(d) into an array of metal islands (white) on a substrate (black). Since in the case considered Ostwald ripening is only efficient for surface coverage of 50% and less [25, 43, 44], we expect its major impact to occur at the stage when the metal coverage decreases below 50%, and start with an approximately 50%-covered substrate as the initial condition. Figure 14 demonstrates typical examples of the evolution of the surface subject to sputtering and Ostwald ripening, starting from the initial pattern in figure 13. Thus, figures 14(a)–(c) present the surface evolution for $\rho_s = 10^3$. In this case metal islands mostly shrink, and their positions do not change significantly until the islands are removed. No significant coarsening is
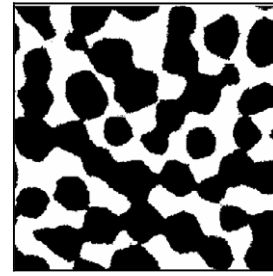
Figure 13. Metal islands on a substrate obtained from the surface pattern in figure 2(d). White is metal, and black is substrate.

evident. For $\rho_s = 10^4$ (figures 14(d)–(f)) shrinkage is still the major factor affecting the size of the metal features that, however, acquire smoother shapes. Although most features do not change their positions significantly, the resemblance to the initial morphology is partially lost. For the case of $\rho_s = 10^5$ shown in figures 14(g)–(i), strong coarsening produces a percolation network with extended features, gradually losing resemblance with the initial pattern in size, shape, and location. At the same time, the metal features seen in figures 14(h) and (i) resemble closely the experimental images for Cu islands on Si substrate shown in figures 9(a) and (b), respectively.

From the examples given in figure 14 it is evident that the impact of the interface coarsening on the metal pattern increases with the kinetic rate ρ_s, and this impact is pronounced only at sufficiently high levels of ρ_s. In [25] we have studied in detail the evolution of the metal features' size[5] λ for model metal patterns on substrates. Figure 15 presents the selected results of relevance for this discussion. Thus, figure 15(a) shows two typical cases of evolution of feature size λ as the function of the duration of sputtering. For $\rho_s = 10^4$ the feature size only decreases throughout the simulation. For $\rho_s = 10^5$, however, metal features increase in size until approximately 3–4 sputter steps per cell are reached, after which sputtering prevails and the features start to shrink. Figure 15(b) shows the maximum feature size reached, $\lambda_{\max}$, from simulations where a significant (more than 10%) increase in size was detected, for various initial feature sizes λ_0. A remarkable property seen in figure 15(b) is that $\lambda_{\max}$ is not sensitive to the initial size λ_0. At the same time, from figure 15(b) it is evident that $\lambda_{\max}$ is related to the kinetic rate ρ_s by $\lambda_{\max} = a\rho_s^{1/3}$. Thus, the value $a\rho_s^{1/3}$ represents a kinetic limit for coarsening in the system considered. This value can be interpreted as a measure of the size reachable by Ostwald ripening under conservative conditions (no sputtering) over a time interval required to execute ρ_s diffusion steps per cell [25].

Figure 15(c) summarizes our numeric results for various values of ρ_s and initial feature sizes λ_0. The figure

---

[5] For the initial pattern with 50% coverage, we define the average feature size λ as the position of the first minimum of the correlation function $C(r, s)$, where $h = 1$ for metal and $h = 0$ for uncovered substrate. Thus, the initial size λ_0 in figures 15(a) and (b) corresponds to half the inter-feature distance d in the network-like patterns generated by normal ion incidence (see section 2). For coverage below 50%, we estimate the size by $\lambda = \xi\sigma/p$ where σ is the total area of the metal features, p is their total perimeter, and $\xi = 2.4$ is an empiric coefficient chosen such to fit the minimum of the correlation function as the coverage approaches 50%.
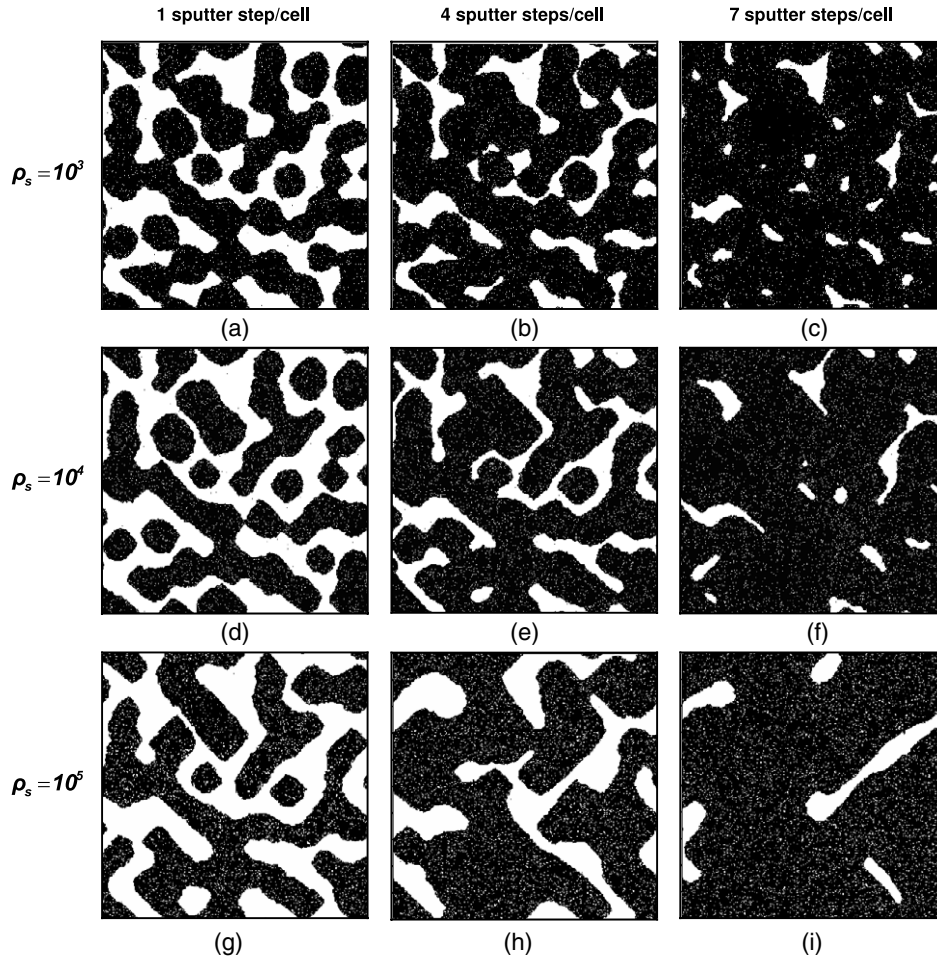
Figure 14. Simulation of the evolution of metal patterns (white) on substrate (black) for various kinetic rates, ρ_s. The images represent 100 nm × 100 nm surfaces.

distinguishes the simulations when a significant coarsening was detected and those when no pronounced coarsening was found. It is evident that the evolution of surface patterns shows two different regimes. The feature size increases significantly only in those cases when $\lambda_0 < a\rho_s^{1/3}$. Otherwise ($\lambda_0 > a\rho_s^{1/3}$) no considerable increase in size occurs.

In the nanofabrication process considered in this paper, the initial feature size λ_0 is defined by the lateral size d of the surface roughness generated by ion bombardment (section 2). For network-like patterns generated under normal ion incidence, $d \approx 2\lambda_0$ by the definition (see footnote 5). Thus for the normal incidence, the condition at which no significant interface coarsening can be expected, reads

$$d > 2a\rho_s^{1/3}. \qquad (1)$$

Since for normal incidence $d \approx 12.1a\rho^{0.22}$ (see figure 6), the condition at which the interface coarsening is avoided is given by

$$\rho_s^{0.33} < 6.1\rho^{0.22}. \qquad (2)$$

Recalling that $\rho_s = 4D_s/J_0Ya^4$ and $\rho = 4D/J_0Ya^4$, the condition is,

$$\left(\frac{D_s}{J_0Ya^4}\right)^{0.33} < 7.0\left(\frac{D}{J_0Ya^4}\right)^{0.22}, \qquad (3)$$

where D_s and D are the metal adatom's diffusivities over the substrate's and metal's, surfaces, respectively. Our analysis has shown that for the ion etching regimes considered in this paper, equation (3) can be replaced by an approximate 'no-distortion' condition, which is simply $\rho_s \ll \rho$. If the ion flux J_0 does not change throughout the entire process, the requirement is $D_s \ll D$. This means that the resistance of metal patterns against the interface coarsening is defined largely by the substrate's material. For the distortions to be avoided, the diffusivity of metal adatoms over the substrate should be low in comparison to their surface self-diffusion coefficients.

In light of this discussion, our experiments described in section 3 can be easily interpreted. Thus, the Cu network patterns generated on glass by normally incident ions seem to not be subject to any significant distortion (figure 8), indicating that the diffusivity of Cu on glass is relatively slow. In contrast, the coarse patterns of Cu on Si (figure 9), and those of Ag (figure 11) can be explained by relatively high surface diffusivities of metal adatoms in these samples.

However, in spite of the expected high diffusivity of Cu adatoms on Si substrates, grazing ion bombardment of Cu films on Si generates well-defined arrays of lines, which are basically similar to those on glass (figure 10). This remarkable resistance of the lines to distortions is related to their geometry, and also
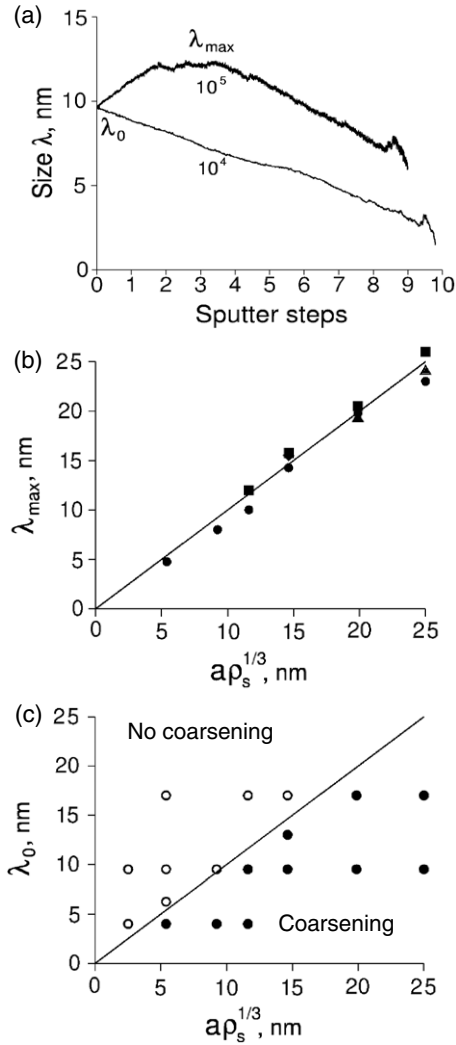
Figure 15. (a) The size of simulated metal islands λ as a function of the number of sputter steps per cell for $\rho_s = 10^4$ and 10^5; (b) the maximum island size λ_{max} as a function of $a\rho_s^{1/3}$ from those simulations where the size increased by more than 10%, for the initial island sizes λ_0 of 4 nm (●), 10 nm (■), 13 nm (♦), and 17 nm (▲); (c) results of simulations for various initial sizes λ_0 and parameters ρ_s. Filled circles indicate simulations where the size increased by more than 10% and open circles indicate simulations where no significant increase was detected. The initial feature size λ_0 in (a) and (c) is related to the average inter-feature distance d by $\lambda_0 = 0.5d$ (see footnote 5). The lines in (b) and (c) show the $a\rho_s^{1/3}$ dependence. Adapted from [25].

reflects the basic trends of the interface coarsening. Thus, for Ostwald ripening to occur, metal adatoms should be able to diffuse throughout the substrate, providing an efficient material exchange between the islands, so that metal features with a lower boundary curvature could grow at the expense of those with higher curvature. The parallel Cu lines block migration of Cu adatoms to remote locations, whereas neighbor lines that can exchange adatoms are similar in shape and local boundary curvature. As a result, a dynamic balance is maintained and the lines do not coarsen. This can also be interpreted as metal lines having a large initial size λ_0 in the longitudinal direction, which prevents their distortion by the interface coarsening.

In conclusion:

- Metal islands formed on the substrates are subject to coarsening through Ostwald ripening, e.g. larger features with fewer corners per unit perimeter grow at the expense of smaller ones. This process requires an efficient migration of metal adatoms over the substrate, providing the adatom exchange between islands.

- If there are obstructions to the adatoms' migration, Ostwald ripening can be insignificant or absent. The origin of these obstructions can be either kinetic (low λ_{max}, slow adatoms' diffusion) or geometric (extended metal features such as lines, or more than 50% metal coverage).

- An interesting outcome is that the cooperative effect of Ostwald ripening and etching has two different regimes depending on the proportion between the lateral size λ_0 of the metal features, and the characteristic size $\lambda_{max} = a\rho_s^{1/3}$. If $\lambda_0 < a\rho_s^{1/3}$, the island's size increases to approximately this value. If sputtering continues further, the islands shrink. Otherwise ($\lambda > a\rho_s^{1/3}$) the islands can only shrink through the process of surface etching.

- For the network-like metal features generated by normally incident ions, the resulting condition of resistance to the interfacial coarsening is $\rho_s^{0.33} < 6.1\rho^{0.22}$, where $\rho_s = 4D_s/J_0Ya^4$ and $\rho = 4D/J_0Ya^4$. For practically relevant process conditions, this is equivalent to a simplified requirement, $D_s \ll D$. Thus, the interface coarsening can be avoided if the metal adatom diffusivity over the substrate D_s is slow in comparison with the diffusivity D on the metal surface. Different adatom diffusivities might explain the different coarsening behavior that we observe experimentally for Cu patterns on glass and Si under normal ion incidence. Thus, the apparent stability of Cu networks on glass is rather of a kinetic origin.

- The observed resistance to coarsening of Cu lines on glass and Si substrates seems to result from both geometric and kinetic factors. Large longitudinal dimensions of the lines block migration of Cu adatoms, and also exceed the maximum achievable feature size λ_{max}.

- The stronger coarsening of Ag features as compared to Cu can be explained by a higher surface diffusivity of Ag adatoms. Although precise data on Cu and Ag diffusion on the glass and Si substrates are unavailable, Ag is known to have a higher diffusivity than Cu [36, 45], which is in line with the behavior that we observe.

A systematic experimental verification of these numeric predictions would be of keen interest. First of all, this concerns the dependencies presented in figures 15(b) and (c). Although the qualitative trends can be predicted with a high level of confidence, the characteristic sizes would depend on the detail of the surface diffusion of adatoms and on their interaction with the metallic islands. Unfortunately, quantitative information on metal adatoms' diffusion over the surface of Si and glass exposed to ion bombardment is, basically, unavailable. Most if not all published research address diffusion at crystalline surfaces such as Si(111) or Si(100), which relevance is questionable because Si becomes amorphized under the ion bombardment [25]. A detailed analysis of the adatom jump

mechanisms over the amorphized non-metallic surfaces still needs to be done. Another point of interest is the extension of the model to account for the adatom jumps uphill to the cluster's terraces, and back from the terraces to the substrate. For poor silicide formers the first process can be expected to prevail, which may somewhat decrease the size of the metal clusters in comparison to the present model predictions. Our expectation is that the results described here would stimulate further brainstorming of the atomic diffusion mechanisms behind the interfacial phenomena defining the quality of IBS nanopatterns.

5. Summary

Ion beam nanostructuring of thin metal films is a unique, very promising, but challenging technique. The surface nanostructures arise as a result of an intricate interplay of several quite complex physical processes. Some of the resulting properties, such as the shape and orientation of the pattern at the surface of a metallic film can be manipulated by varying the angle of incidence and the flux rate of the ion beam. Others, such as the stability of the metal pattern on a substrate of another material, depend largely on the metal/substrate combination. Further development of this methodology requires a meticulous understanding of the mechanisms of sputtering and coarsening involved.

From our results it appears that IBS nanostructuring of thin metallic films has two distinctly different stages, where the mechanisms and outcomes of coarsening are also totally different. At the initial stage, when a continuous metallic film is exposed to ion beam sputtering, the surface pattern created by the kinetic instability coarsens mainly by coalescence of the surface features. The coalescence, which involves a stochastic drift of the features over the surface and their merging together, is known to be a slow process [44]. As a result, the kinetic mechanism of surface nanostructuring seems to dominate over coarsening. As we have demonstrated in section 2, the surface patterns only coarsen moderately over the initial stages of sputtering, after which the features' size stabilizes. The positional correlation of the surface features is not destroyed by coarsening at this stage. Moreover, for the arrays of ripples formed at grazing ion incidence, coalescence is rather a favorable process, since it eliminates defects making the ripples more uniform. The size, shape, and orientation of the surface pattern are controllable by the bombardment conditions.

However, at the stage when metallic islands are formed on a substrate of a different material, another mechanism of coarsening becomes important, which tends to decrease the excess energy of the island's boundaries. This occurs through the Ostwald ripening, which usually is relatively fast [43, 44]. As a result, some of metal patterns are transformed into coarse networks or islands, whose position, size, and shape may have little in common with the initial IBS-generated structure. Examples of this are given in section 3. For the surface nanopattern to not be distorted, Ostwald ripening should be obstructed. Fortunately, the concurrent process of sputtering and coarsening has kinetic limitations over the impact of Ostwald ripening, as discussed in section 4. The kinetic obstruction of interface coarsening seems to occur in the case of nanoscale Cu dots and networks on glass.

The arrays of metal lines are less sensitive to distortions by the interface coarsening than networks or arrays of dots. Moreover, as already discussed, coarsening of metal ripples at the early stages of sputtering is of a positive influence on the uniformity of the pattern. This unique resistance against distortions makes fabrication of the arrays of nanoscale metal lines on substrates a realistic and very attractive application for the two-stage process of IBS nanostructuring.

For a controllable fabrication of metallic nanodots or networks on substrates to be fully realized, new solutions to obstruct the interface coarsening need to be found, which would require intensive research both numerically and experimentally. Thus, the variety of atomic diffusion mechanisms and their impact on the IBS nanopatterning should be addressed in detail. Another rather technical challenge yet to be solved is an efficient method to detect the stage when the surface pattern has reached the metal/substrate interface, and the ion etching should be stopped. To achieve a well controllable fabrication process, the removed depth should be identified with atomic scale precision. One solution that we have used was monitoring the surface composition by XPS [25]; however, alternative cost-efficient solutions compatible with the standard dry etching equipment for VLSI fabrication would be desirable. To conclude, the process of IBS fabrication of surface nanostructures has strong potential for further development, albeit requiring some research and technical challenges to be solved successfully. Looking forward, one can predict considerable room for future numeric and experimental studies, along with engineering developments.

Acknowledgments

References

[1] Whitesides G M and Grzybowski B 2002 *Science* **295** 2418
[2] Bradley R M and Harper J M E 1988 *J. Vac. Sci. Technol.* A **6** 2390
[3] Fasco S, Dekorsy T, Koerdt C, Trappe C, Kurz H, Vogt A and Hartnagel H L 1999 *Science* **285** 1551
[4] Carter G 2001 *J. Phys. D: Appl. Phys.* **34** R1
[5] Valbusa U, Boragno C and Buatier de Mongeot F 2002 *J. Phys.: Condens. Matter* **14** 8153
[6] Chan V L and Chason E 2007 *J. Appl. Phys.* **101** 1231
[7] Cuerno R and Barabási A-L 1995 *Phys. Rev. Lett.* **74** 4746
[8] Rusponi S, Costantini G, Boragno C and Valbusa U 1998 *Phys. Rev. Lett.* **81** 2735
[9] Carter G 1999 *Phys. Rev.* B **59** 1669
[10] Park R, Kahng B, Jeong H and Barabási A-L 1999 *Phys. Rev. Lett.* **83** 3486

[11] Makeev M A, Cuerno R and Barabási A-L 2002 *Nucl. Instrum. Methods* B **197** 185

[12] Hartmann A K, Kree R, Geyer U and Kölbel M 2002 *Phys. Rev.* B **65** 193403

[13] Stepanova M, Dew S K and Soshnikov I P 2002 *Phys. Rev.* B **66** 125407

[14] Bobek T, Facsko S, Kurz H, Dekorsy T, Xu M and Teichert C 2003 *Phys. Rev.* B **68** 085324

[15] Karmakar P and Ghose D 2004 *Nucl. Instrum. Methods* B **222** 477

[16] Karmakar P and Ghose D 2004 *Surf. Sci.* **554** L101

[17] Stepanova M and Dew S K 2005 *Mater. Res. Soc. Symp. Proc.* **849** 35

[18] Stepanova M, Dew S K and Soshnikov I P 2005 *Appl. Phys. Lett.* **86** 073112

[19] Yewande E O, Hartmann A K and Kree R 2005 *Phys. Rev.* B **71** 195405

[20] Yewande E O, Kree R and Hartmann A K 2006 *Phys. Rev.* B **73** 115434

[21] Munoz-Garcia J, Castro M and Cuerno R 2006 *Phys. Rev. Lett.* **96** 086101

[22] Stepanova M and Dew S K 2006 *J. Vac. Sci. Technol.* B **24** 592

[23] Mishra P and Ghose D 2006 *Phys. Rev.* B **74** 155427

[24] Mishra P and Ghose D 2008 *Nucl. Instrum. Methods* B **266** 1635

[25] Stepanova M, Dew S K and Karpuzov D S 2005 *J. Appl. Phys.* **97** 083536

[26] Rimberg A J, Ho T R and Clarke J 1995 *Phys. Rev. Lett.* **74** 4714

[27] Park K H, Ha J S, Yun W S, Shin M, Park K W and Lee E H 1997 *Appl. Phys. Lett.* **71** 1469

[28] Bruggemann M, Masten A and Wissmann P 2002 *Surf. Sci.* **406** 294

[29] Lombardo S, De Salvo B, Gerardi C and Baron T 2004 *Microelectron. Eng.* **72** 388

[30] Baron T, Gentile P, Marnea N and Mur P 2001 *Appl. Phys. Lett.* **79** 1175

[31] Ciraci S, Buldum A and Batra I P 2001 *J. Phys.: Condens. Matter* **13** R573

[32] Liu Z, Wang H and Li H 1998 *Appl. Phys. Lett.* **72** 1823

[33] Portales H, Saviot L, Duval E, Fujii M, Hayashi S, Del Fatti N and Vallée F 2001 *J. Chem. Phys.* **115** 3444

[34] Kuwata H, Tamaru H, Esumi K and Miyano K 2003 *Appl. Phys. Lett.* **83** 4625

[35] Stepanova M and Dew S K 2002 *J. Appl. Phys.* **92** 1699

[36] Giesen M 2001 *Prog. Surf. Sci.* **68** 1

[37] Siegert M and Plischke M 1994 *Phys. Rev.* E **50** 917

[38] Zinke-Allmang M, Feldman L C and Grabow M H 1992 *Surf. Sci. Rep.* **16** 377

[39] Bray A J 1994 *Adv. Phys.* **43** 357

[40] Thornton K, Ågren J and Voorhees P W 2003 *Acta Mater.* **51** 5675

[41] Venables J A, Spiller G D T and Hanbücken M 1984 *Rep. Prog. Phys.* **47** 399

[42] Ratch C and Venables J A 2003 *J. Vac. Sci. Technol.* A **21** S99

[43] Zhdanov V P and Kasemo B 1999 *Surf. Sci.* **437** 307

[44] Lo A L and Skodje R T 2000 *J. Chem. Phys.* **112** 1966

[45] Chou S H, Freeman A J, Grigoras S, Gentle T M, Delley B and Wimmer E 1988 *J. Chem. Phys.* **89** 5177